SYSTEM DEVELOPMENT FOR MARS ENTRY IN SITU RESOURCE UTILIZATION

Svetozar Popović[(1)], Robert W. Moses [(2)], Leposava Vušković[(3)]

[(1)] *Old Dominion University, 4600 Elkhorn Avenue, OCNPS, 306, Norfolk, VA 23529, USA, Email: spopovic@odu.edu*
[(2)] *NASA Langley, 1 N Dryden St. (MS489), Hampton, VA 23681, USA, Email: Robert.w.moses@nasa.gov*
[(3)] *Old Dominion University, 4600 Elkhorn Avenue, OCNPS, 306, Norfolk, VA 23529, USA, Email: lvuskovi@odu.edu*

ABSTRACT

In this paper we report the on the state of effort to characterize Mars entry plasma as a potential work fluid for on–board power generating systems, and a chemical reactor medium for oxygen generation. The use of Martian entry plasma can be augmented using the concept of regenerative aerobraking may offer a revolutionary approach for in situ power generation and oxygen harvesting during the exploration missions. The on-board power conversion system concept is based on a network of lightweight magnetohydrodynamic power generators developed in NASA LaRC and at ODU. The system consist of several subsystems that would address the Oxygen production and storage, utilize MHD cooling of thermal shield, provide power by MHD conversion for fluid cooling subsystem and heat redistribution to a resistive load to the rear of the spacecraft. Detailed conceptual description of some of these systems is the subject of present talk.

INTRODUCTION

The objective of the recently proposed "regenerative aerobraking" technology is to capture some of the abundant available kinetic energy of a spacecraft as it enters the Martian atmosphere (10-1000 gigajoules) that would otherwise be wasted [1]. The basic idea of this approach is to make use of the ionized gas and intense heat generated in the vehicle's entry plasma for power conversion, effective heat flux distribution, and oxygen production. Fundamental magnetohydrodynamic (MHD) physics principles support the concept of placing magnetic field within the plasma in order to generate usable electrical currents. We note that the term in situ resource utilization (ISRU) has been mostly attributed to Martian surface efforts, where power constraints rendered use of plasma ineffective, although feasible. Most MHD concept devices require alkali seeding to achieve the necessary level of electrical conductivity of the flowing ionized gas for MHD power conversion. Electrical conductivity of direct entry and aerobraking plasmas is already high enough and does not require any seeding.

The paper is organized as follows. First we describe briefly the properties of the Martian entry plasma for the case of direct entry. Aerobraking and aerocapture maneuvers also involve still substantial mechanical energy loss in deceleration, and generate highly ionized entry plasma and the studies of their parameters show that the same principles outlined in this paper could be applied to the systems utilizing the direct entry plasma. In the second section we describe the magnetohydrodynamic power generator unit and its use as the energy source to provide the necessary energy for the system operation.

1. MARTIAN ATMOSPHERIC ENTRY PLASMA CHARACTERISTICS

There are several possible maneuvres of deceleration at Mars. Two of them have been demonstrated – direct entry[2,3] and aerobraking [4,5], and the third, aerocapture, has been intensively studied [6,7]. Each maneuver has separate hypersonic characteristics as they pass from the hyperbolic to elliptical trajectories. Shock parameters in front of the entry vehicle change substantially and that affects the entry plasma. NASA's Pathfinder and Viking Landers found that the Martian atmosphere below 100km was primarily composed of CO_2 (95.32%) with minor components of N_2 (2.7%) and Ar (1.6%). In addition, the landers observed the free stream density, pressure, and temperature during the entry phase into the atmosphere. This phase begins at approximately 180 km above the surface and lasts until the parachutes are deployed for landing, around 9 km, with a total elapsed time of approximately 120 s. The free stream temperature measurements from the Pathfinder Lander and Viking Landers 1 & 2 are presented in Fig. 1. From the figure, we observe that the temperature is very high in the upper atmosphere which most likely is caused by solar radiation. The temperature then decreases with decreasing altitude reaching a minimum at 80 km. According to Schofield *et al.* [8], this temperature minimum may be due to a superposition of

waves, such as thermal tides. These tides will propagate from the lower atmosphere to higher altitudes with increasing amplitude. After 80 km the temperature once again begins to increase till it reaches an average of about 220 K at the surface.

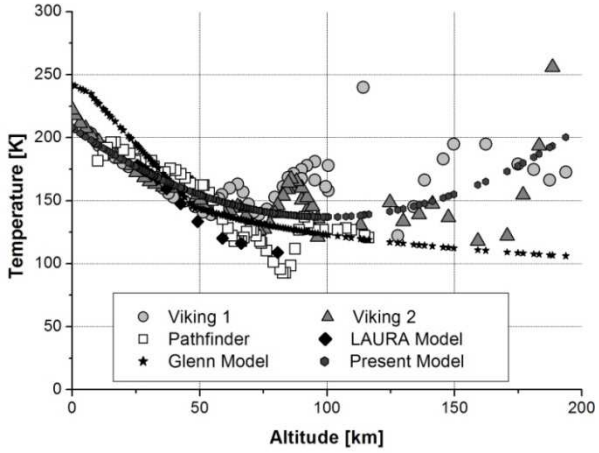

Fig. 1. Temperature distributions in the Martian atmosphere from Viking Landers 1 & 2, Pathfinder Lander, the NASA Glenn model, an input to LAURA model calculations, and our present model [9].

By reconstructing the entry trajectory of the Martian probes, when we use the present model we are able to develop an accurate portrait of all the atmospheric phenomena faced by them. For instance, Viking Lander trajectory at various stages covered latitudes between 15 and 22 degrees, approximately and longitudes between 300 and 310 degrees east. Mars Pathfinder landing site was at 23^{o}N and 338^{o}E. All landings were made during the daytime.

There is additional uncertainty posed by the latitudinal and longitundinal atmospheric conditions, by seasonal and diurnal variations of temperature, For instance, data from Thermal Emission Spectrometer (TES) suggest significant latitudinal dependence of free stream temperature as shown in Figure 2. Mean temperature at the longitude of 270^o during southern hemisphere summer show relatively uniform behavior up to about northern latitude of 30^o. Northern winter is presented by a substantial reduction of temperature above 30^o.

In order to effectively estimate electron density and gas composition for Martian atmospheric entry plasma (MAEP), we must construct a simple model for the shock region in front of each probe during entry. For this model certain assumptions must be made: (1) the gas mixtures generated during entry are thermodynamically perfect gases, (2) ionization occurs instantly behind the shock front, (3) the gas mixtures are constant in the boundary layer behind the shock front, and (4) gas parameters are defined by the free stream parameters and the relations across the shock. From these assumptions, we are able to calculate the shock parameters, such as the temperature

$$T_2 = T\left\{1+\frac{2(\gamma-1)}{(\gamma+1)^2}\frac{\mathrm{A_M}-1}{\mathrm{A_M}}\left[\gamma \mathrm{A_M}+1\right]\right\} \quad (1)$$

where $\mathrm{A_M} = \mathrm{M}(T)^2 \sin^2\beta$, β is the oblique shock angle, and T is the atmospheric temperature from Fig. 1. Employing Eq. (2) we calculated the temperature across the shock front and present these results in Fig. 4. We observe that the temperature reaches a peak average value of about 36000 K, 19000 K, and 13000 K for the Pathfinder, MER Opportunity, and Viking Landers, respectively. These maximum values occurred between 50 and 60 km above the surface. The shaded regions give us a range of values for the temperature. For example, the Pathfinder Lander has a peak temperature of 36000 K ± 2500 around 60 km. At higher altitudes all the distributions become wider since the atmosphere becomes less dense. Uncertainty due to latitudinal variation of temperature is relatively low in the regions near equator, which reflects relatively minor error at low altitudes.

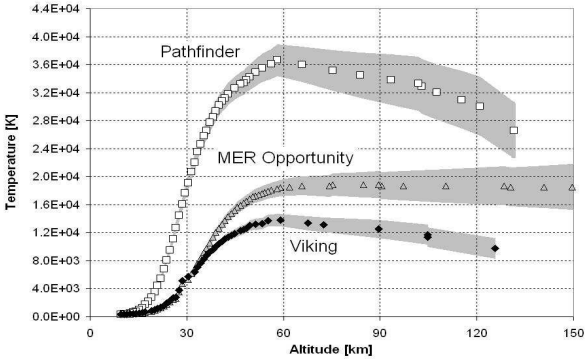

Fig. 2. Temperature across the shock layer in the MAEP. The shaded region is due to the uncertainties of the measured free stream temperature data [9], which reflects global and latitudinal variations of probe trajectories.

Martian air flow around the spacecraft can be divided into two distinct regions that have various level of equilibrium conditions. First, free atmosphere at high altitudes is known to be weakly ionized. In fact, spacecraft passes through a quite dense ionosphere, which extends above 300 km. Measured vertical electron and major ion density distribution in the altitude range above 100 km is shown in Figure 3. Most of ionization comes from solar UV radiation. This is confirmed by the fact that the peak electron density depends on solar zenith angle, and by strong observed diurnal variations. However, the ionosphere still exists in the dark side, and there a high level of ionization is seen even at large zenith angles (70-80^o). Explanations could include a possibility of large amount of energy stored by photo-excitation and

cascade processes in the vibrationally and electronically excited states of O_2 and CO_2 and in the much stronger ionizing radiation activity in the diluted atmosphere.

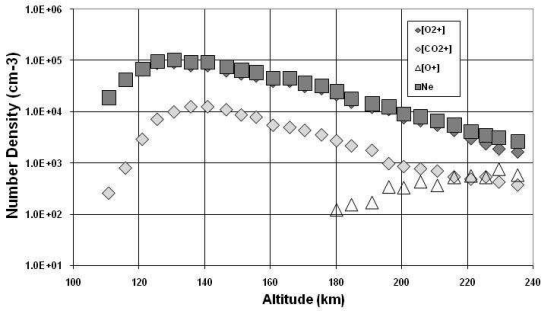

Fig. 3. Measured free stream electron and ion density variation with altitude.

High densities of charged particles are combined with relatively low neutral density, so that in the same altitude range the degree of ionization varies from 0.01 at 200 km to ~10^{-7} at 100 km. Therefore, the free stream conditions are those of a diluted weakly ionized gas in the state of strong non-equilibrium with the average electron energy exceeding by two orders of magnitude the gas temperature.

Second is the zone of interaction between the entry plasma and the ionospheric gas. Presence of charge particles from the both sides of the shock add to UV radiation from the dense entry plasma and open a new set of processes that contributes to formation of ionization wave behind the shock. In this zone the equilibration of charged particle energy takes place and kinetic description is a valid approach.

Characteristics of the free Martian atmosphere are still being studies and detailed properties are not known. It is know quite certain that most of required seeding in the low velocity (5 km/s) maneuvers has been actually provided naturally, by the space charge in the Mars ionosphere, and by photoionization processes provided by the forward radiation of the vehicle bow shock.

2. MHD POWER GENERATOR

Magnetohydrodynamic generator transforms the energy of the plasma into electric power. The MHD generator is particularly well suited for those applications involving high power, high temperature, or both [11]. As illustrated in Figure 3, aerobraking provides both. The material within the MHD generator ionizes under these conditions. When the electrons and ions encounter a magnetic field, they are forced to the electrode corresponding to their polarity. The path of least resistance for the electron is to travel onto the anode, along the wire, through the load to recombine with the ion on the cathode.

In the context of regenerative aerobraking, two types of MHD power generators have been studied. First, the traditional *internal* MHD generator, shown in Figure 4, consists of a duct down which the gas flows, an arrangement of coils that produce a magnetic field across the duct, and electrodes on either side that carry off the current. The power output is a function of electron number density (N_e), the square of the velocity (u) and the magnetic field strength (B), the crosssectional area of the duct (A_c), and the interaction length (L_i). In general, internal MHD generators have an efficiency of about 25%. The advantage of the internal MHD generator is that most of the ionized plasma passes through the duct and interacts with the magnetic field and the electrodes. One challenge for implementing the internal concept within a spacecraft is that temperature-sensitive components need to be shielded from the hot gas in the channel.

The second type of MHD power generator, which was conceived during this project, does not contain a duct. Coined an *external* MHD power generator, this new type takes advantage of the boundaries formed by the outer mold line of the spacecraft and the shock layer just ahead of the spacecraft. In concept, magnets just behind the outer wall of the spacecraft project the magnetic field into the flow field to force the ions to hit the electrodes protruding out of the surface toward the shock layer. The advantage of the external concept is that no hot gases enter the spacecraft. The challenge of this concept centers around the material selection for the electrodes, and the thermal protection system on the front of the spacecraft.

As mentioned earlier, multi-pass orbits about Mars allow longer time periods to extract power. The intent of regenerative aerobraking is to provide resources to benefit operations on Mars after maximizing the time spent in the atmosphere generating power and extracting other resources, like oxygen. This entails multiple passes through the atmosphere, at velocities to produce sufficient electron number densities, followed by the descent and landing. The terminology of E^{i}DL is used to define this orbit approach, where "i" denotes the number of passes (entries) before the eventual descent (D) and landing (L). The number of passes can be varied by changing the ballistic coefficient. To generate these different cases, the ballistic coefficient was varied by changing the presumed surface area of the vehicle. For the first case, the area is presumed at 7 m^2, and is dropped by one-half for each subsequent case. The resulting orbits for three cases of E^{i}DL are i = 3, 7, and 11. The average entry properties are as follows: 1) velocity around 4.5 km/sec; 2) average atmospheric density is

$8x10^{-5}$ kg/m^3; and 3) average time in the atmosphere is 550 seconds per orbit.

For the multi-pass cases for i = 3, 7, and 11, respectively, the total times spent in the atmosphere are 1881 seconds, 4390 seconds, and 7400 seconds, respectively. Although the velocities for these cases are just below 5 km/sec, resulting in lower electron number densities than the direct entry case, the MHD power can be boosted by atmospheric seeding the flow. Based on these estimates, the energy that can be generated per orbit is approximately 500 megajoules per 1 m^2 of external MHD generator area. For each case, the number of passes can be increased by compensating for the atmospheric drag occurring during each pass. One way to compensate for the drag is to perform a Δv on the order of tens of meters per second at apoapsis following each pass through the atmosphere.

The proof-of-concept for this first step of extracting energy from the entry plasma has recently been reported[10]. A relatively simple laboratory supersonic plasma flow system was developed (See Figure 4), operating at a flow velocity of M = 2.1 with gas composition and conditions simulating the Martian atmosphere. A schematic of the model MHD generator is shown in Figure 6. Compact $SmCo_5$ permanent magnets were used in the experiments with magnetic field strength of 0.1T. The MHD generator produced a current of 150 mA at a voltage between the current-collecting electrodes of 3 V. The maximum power generated was close to 0.5 W, which converts to a power density of 0.1 W/cm^2.

The converted MHD power density scales as the square of flow velocity and the square of the magnetic field strength at a given pressure. The Martian entry plasma flow velocity is approximately M = 20. Therefore, using stronger magnets of about 1T field strength, the power density generated at Martian entry is expected to be at least of the order of 1MW/m^2, and the harvested energy would be at least of the order of 100 MJ/m^2.

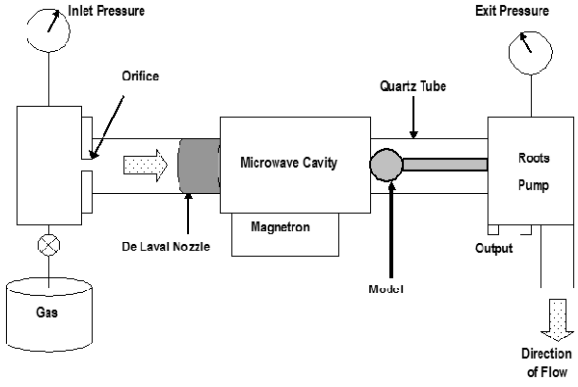

Figure 4. Scheme of the supersonic flow discharge experimental apparatus external MHD generator model studies.

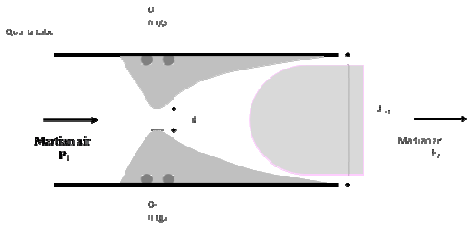

Figure 5. Sketch of the microwave-transparent convergent-divergent (de Laval) nozzle showing the plasma region and the direction of flow

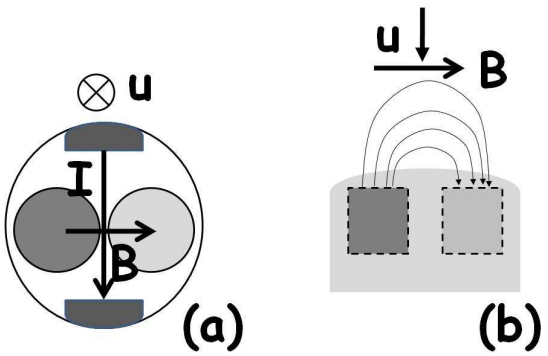

Figure 6. Conceptual scheme of the MHD power generator model: (a) front view, and (b) side view. Two permanent magnet coupons are imbedded with opposite polarity in a ceramic disc. The magnets generate the necessary magnetic field that couples with the plasma flow to form electric current that is collected by two conductive plates

Lateral magnetic field distribution in front of the permanent magnets indicates that the model MHD power generator could achieve conversion at a distance of 2 cm from the face of the permanent magnet coupons, or about 1 cm ahead of the Outer Mold Line, with remaining 1 cm spent on thermal protection of the magnets.

MHD power generated in a MHD generator is given by [11]

$$P_{\max} = \frac{1}{4}\sigma_{eff} v^2 B^2 \qquad (2)$$

where v is the direct component of flow velocity, B is the lateral component of the magnetic field strength from the on-board magnets, and the effective electrical conductivity σ_{eff} is reduced from the d.c. electrical conductivity by the ion slip factor that depends on the configuration of the electrodes.

The extractable MHD energy density was estimated from the available data on Martian entry [10] and shown in Figure 7.

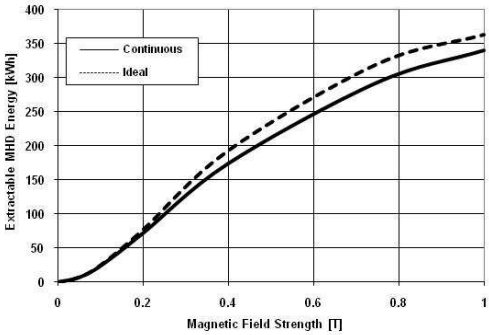

Figure 7. Estimated maximum extractable MHD energy from the Mars Pathfinder entry trajectory.

As seen from Figure 7, the extractable MHD energy per 1 m^2 of probe area depends on the magnetic field strength so that, for instance, at B=0.2 T its value is about 250 MJ, depending on the electrode design. Due to several adverse effects, including but not limited to the ion slip, the scaling of power with the square of lateral magnetic field strength is limited to the low magnetic field intensity. In the laboratory supersonic discharge plasma in Martian stimulant gas mixture, we were generating electron density of about 5×10^{11} cm^{-3} and the flow speed of about M = 2. Average lateral magnetic strength was of the order of 0.1 T. For those conditions the model MHD generator unit with front surface of 3 cm^3 was capable of producing 0.45 W, or 1.5 kW/m^2. When it is scaled up to the direct entry conditions the estimated extracted energy would be about 40 kWh. The estimated scaling takes into account the unoptimized constructional filling factor of permanent magnets.

Validation of MHD conversion concept in a supersonic microwave flowing afterglow apparatus, with an external MHD generator required an innovative diagnostic approach. Conventional optical methods for flow characterization could not be applied due to too low static pressure range (0.5-3 Torr). More elaborate modern optical techniques required equipment that was unavailable or underdeveloped. Therefore, we had to rely on optical emission spectroscopy not only to determine plasma parameters, but also to characterize the flow. Accumulation of electronically excited states near the shock layer and the consequent increase of spectral line intensity is a convenient effect for the development of a non-intrusive method for shock wave characterization in the flow of rarefied ionized gas. This fact has remained unnoticed due to the fact that most of the experiments in weakly ionized gas were performed using a traveling shock wave. Very few experiments with detailed diagnostics have been reported so far on stationary shock.

Measurement of the collected current presented another challenge, especially in the case when bias was applied. Any direct measurement of electric parameters is at least intrusive if not outright impossible. Therefore, we opted for development of an optical-coupling technique, using the correlation between the current through a LED diode and the light emission. Absence of current threshold in the light source emission characteristics combined with the wide dynamic range of the PMT detector, allowed for the calibration of current over several orders of magnitude, from microampere to milliampere range.

3. MARS ENTRY ISRU SYSTEM

Having previously demonstrated the basic concept of MHD power conversion from plasma flow, in this section we will address the challenges for on-board generation of MHD power and for making use of this power. Specifically, the objectives for this work are to develop and to seek to validate the concepts for following regenerative aerobraking subsystems:

1) Modular MHD generator matrix;
2) Electrical current distribution unit;
3) Active thermal shield cooling and entry communication black-out mitigation subsystem;
4) Autonomously powered subsystem for active fluid-cooling of temperature sensitive components;
5) Resistive load network for heat redistribution over the spacecraft;
6) Oxygen harvesting and separation unit; and
7) Rigid, thermo-resistant inflatable container for oxygen/carbon dioxide storage**.**

1) *Modular MHD generator matrix*

In the proposed scheme, permanent magnets will be organized in array modules together with the collecting (binning) electrodes as indicated in Figure 8a. Electrically, the individual generator units will be connected in parallel. The modular structure will be placed along meridian lines below the thermal shield.. The main tasks are to design the modules so that the converted power is multiplied proportionally, to determine the modular current output, and to determine the spacecraft surface layer with temperature below the magnet's Currie point. In a separate effort, the use of lightweight electromagnets would be examined and included in the conceptual designs.

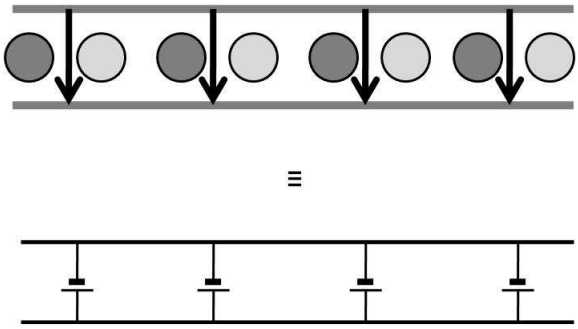

Figure 8a. Modular concept of the MHD generator system. North poles of permanent magnets are labeled in dark grey, and south poles in light grey. Black arrows indicate the current direction.

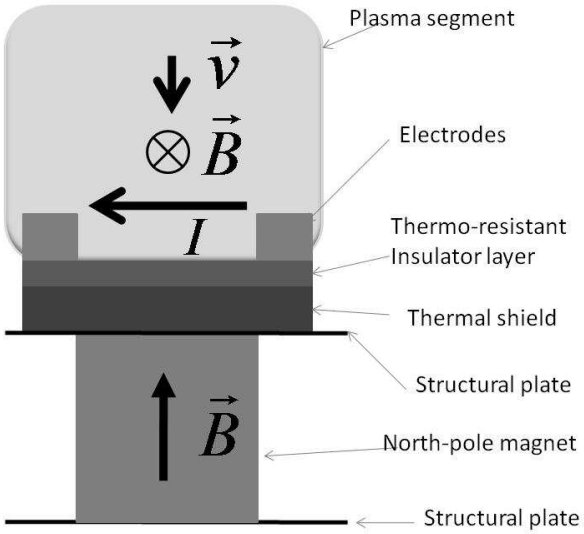

Figure 8b. Sketch of the left side view of the MHD generator module. Dimensions are not to scale.

Concept of the modular structure is illustrated in Figure 8b. It is conceived that the magnets will be positioned behind the thermal shield layer, and the collection electrodes will face the plasma. *No seeding* for enhancement of conductivity is assumed, since the estimates of electrical conductivity in Martian entry plasma warrant ample current collection [10].

(2) Electric current distribution unit

The electric current distribution unit will accept current from the MHD generating system and control the distribution of electric power over the spacecraft as schematically illustrated in Figures 8a,b. Its experimental design will initially implement battery power with the same power rating as the scaled up module power based on the experimentally defined value of 0.15 W/cm^2 at M = 2 flow and magnetic field strength of 0.1 T. The proportionality of the converted power to the square of flow velocity and the square of magnetic field strength, as well as the scaled electrical conductivity will be used to determine the design parameters.

(3) Active thermal shield cooling and entry communication black-out mitigation subsystem

For this complex and important subsystem, we will develop concepts and components that exploit the considerable opportunity to direct the spatial organization of the entry plasma using locally controlled MHD power conversion. The strength of the ionization sheath that encapsulates the spacecraft can be greatly reduced in specific areas as electrons and ions are redirected by the magnetic field and harvested at the electrodes. Directing the spacecraft's transmission signal through these areas of reduced ionization, especially toward the back of the vehicle, may enable communications during the entire entry. Additionally, the feasibility of a similar approach will be evaluated to stimulate future work in the transmission of power off the spacecraft to a receiver, where it can be stored or used elsewhere. Currently, no assets exist on Mars or its moons to allow this option.

(4) *Autonomously powered subsystem for active fluid-cooling of temperature sensitive components*

Current thermal protection systems are sized by regulating the temperature at the bond line between the heatshield and the backing structure that provides structural stability to the aeroshell and payload. The bond line near the stagnation region of the heat shield is most at risk. Making use of the power generated by MHD conversion, it may be feasible to provide active cooling to this region. A cooling fluid (such as liquefied gases that do not require cryogenics to maintain) could be pushed through a capillary system that runs near the stagnation region and then to cold parts of the spacecraft that can absorb the heat. Thus, the thermal load that is normally concentrated near the stagnation region may be spread over a larger region to reduce the thermal stresses on the bond line near the stagnation region.

(5) *Resistive load network for heat redistribution over the spacecraft*

The resistive load network serves to dissipate the unused power generated by the MHD module. Its design is based on the predefined requirements of the heat distribution over the spacecraft and the technology

of the lightweight resistive loads and lightweight current connectors. The network includes distributed load switches and interlocks that allow implementation of automatic control of power distribution. The network design naturally depends on the availability of adequate space and mass load in the current spacecraft architecture.

6) *Oxygen harvesting and separation unit*

The elevated temperatures of aerobraking at Mars temporarily free oxygen from the carbon dioxide in the plasma stream. As illustrated in Figure 9, for direct entry at Mars, the amount of oxygen in the stagnation region is considerably greater than any of the other molecular species found there. In the region ahead of the spacecraft, oxygen makes up roughly 50 percent of the mole fraction, followed by carbon monoxide comprising around 30 percent. Recognizing this feature initiated a survey of oxygen filtration technologies, which led to a process called solid oxide electrolysis. For direct entry at Mars, the amount of oxygen in the stagnation region is considerably greater than any of the other molecular species found there. A survey of oxygen filtration technologies include several candidates: (i) vacancy diffusion through nano-crystallite solid oxide electrolytes, (ii) selective oxygen diffusion through silver, and (iii) oxygen separation through erbia stabilized bismuth. Besides, a number of polymer and ceramic oxide materials that are currently used in the fuel cell technologies may serve in the oxygen preprocessing phases.

It has been known for decades that when the cubic phase of ZrO_2 is doped by Y_2O_3 the concentration of oxygen vacancies in the cubic crystallite is increased, which enhances selectively oxygen ion mobility. The material is usually called Yttria Stabilized Zirconia (YSZ) and has been widely used as a solid electrolyte material in solid fuel cells or oxygen sensors. Early Mars ISRU research activity considered this material as the primary candidate for oxygen separation after thermal dissociation of carbon dioxide [12,13].

The knowledge of YSZ and its properties have been developed in several aspects since. It was found that the diffusion of oxygen is orders of magnitude in the interfaces of the nanocrystalline ZrO_2, that the enhancing effect can be obtained by increasing the number of interfaces, and that the tensile strain could enhance oxygen diffusivity in YSZ by another several orders of magnitude [14-16]. Development of the proposed oxygen separation system for oxygen harvesting during aerobraking, or aerocapture maneuvers could contribute to further improvement of this material.

The oxygen flux through a solid electrolyte slab in x direction is given by Fick's law [15]:

$$\text{oxygen flux} = -D\frac{\partial N}{\partial x} = \kappa(N_{container} - N_S) \qquad (3)$$

where D is the total composite diffusivity of oxygen, N(x) is the oxygen number density, κ is the complex quantity defining oxygen surface exchange on the interface between plasma and solid electrolyte, $N_{container}$ is the number density of (molecular) oxygen in the container, and N_S is the number density of oxygen at the exposed surface of the electrolyte. According to [15], the electrolyte composed from nanoscale grains exhibits simultaneously two types of oxygen diffusivities, diffusivity through vacancies between and inside the grain structures, D_V, and the diffusivity through the grain boundaries, D_B. Total composite diffusivity is then given by

$$D = (1 - f)D_V + fD_B \qquad (4)$$

where $f = 2\delta/d$ is the volume fraction of grain boundaries, $\delta \approx 0.5$ nm is the grain boundary, and $d \approx 100$ nm, is the grain diameter. Although the volume fraction is of the order of 0.01, boundary diffusivity is found to be the dominant mechanism leading for an order of magnitude increase in the composite diffusivity D.

Measurements using tracer oxygen ion [15] resulted in a more quantitative information on the oxygen flux through YSZ. The necessary diffusivities are well fitted by the Arhenius plots

$$\boldsymbol{D_V = D_{V0}e^{-\frac{H_V}{kT}}} \qquad (5)$$

$$\boldsymbol{D_B = D_{B0}e^{-\frac{H_B}{kT}}} \qquad (6)$$

where the diffusivity constants are

$$\boldsymbol{D_{V0} = 8.0 \times 10^{-7}\, m^2/s},$$

and

$$\boldsymbol{D_{B0} = 2.0 \times 10^{-5}\, m^2/s}.$$

where $\boldsymbol{H_V = 1.11\ eV}$ is the activation enthalpy for volume diffusion, and $\boldsymbol{H_B = 0.91\ eV}$ is the activation enthalpy for grain boundary diffusion. These values are for 7-15% molar content of Y_2O_3. At lower values of %mol the diffusivity was reported lower [17].

Oxygen surface exchange coefficient κ is defined by [15]

$$\boldsymbol{\kappa = 1.4 \times 10^{-2} e^{-1.13\ eV/kT}\ m/s}. \qquad (7)$$

Oxygen diffusivity through YSZ may depend strongly on the tensile strain. Kushima and Yildiz [16] have calculated that the highest enhancement of diffusivity in 9%-YSZ compared to its unstrained state

is 6.8×10^3 times at 4% strain and at 400 K. At higher temperature the effect falls exponentially, to about 35 at 1000K. According to our estimate, given in Figure 9, the tensile strain effect substantially modifies temperature dependence of total diffusivity. If proven and validated this property may lead to the enabling technology for oxygen separation.

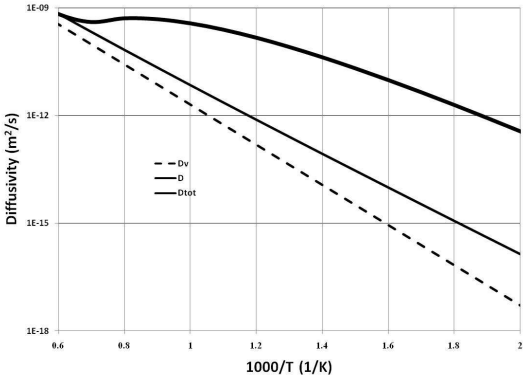

Figure 9. Diffusivity of oxygen through yttria stabilized zirconia: volume diffusivity (dashed line); diffusivity with addition of nanocrystallite interface effect (solid line); total diffusivity of 4% strained material (thick solid line).

Most of the research effort on these ionomers have been devoted to only a small number of materials, notably the ethylenes, styrenes, rubbers, and those based on poly(tetrafluoroethylene). Nafion® is one such example of a poly(tetrafluoroethylene) based ionomer. From its development by DuPont in the 1960s, =it has etched applications in liquid and gas separations, fuel cells, and the chlor-alkali industries. Because of its superior combination of thermal and chemical resistance, ion-exchange properties, selectivity, mechanical strength, and insolubility, nafion is rather popular material for fuel cell membrane design.

Traditional use of quartz frit is to hold catalysts during the chemical processes involving volatile materials. Also, we have suggested quartz frit as a high-temperature preconditioning device for our RF discharge-based dust filtration system. However, in our work on production of $O_2(^1\Delta)$ we have successfully used quartz frit to capture water molecules and OH radicals [18], although it decreased by 50% the flow rate of the system. By analogy, CO_2, CO and O_3 should have much lower permeation rate through quartz frit than oxygen and therefore should have a favorable extracting characteristics. We are currently preparing testing the material in the context of a different program and the results of testing will be available before decision on this project is made.

Dense erbia-stabilized bismuth oxide has been a very promising ion conductor. In a composite containing Ag it has superior oxygen permeability at lower temperatures compared to YSZ [19]. Its operating temperature range is between 900 K and 1100 K. Oxygen permeation flux is close to 10^{17} $cm^{-2}s^{-1}$ for a 230 μm membrane at temperature 1025 K and pressure of about 42.5 Torr [19]. Part of the reason is in the fact that bismuth oxide conducts oxygen molecular ions as opposed to YSZ, which conducts atomic oxygen ions. Therefore, much of attention in the future oxygen separation studies will be devoted to this and similar compounds.

Doped perovskite ($La_{1-x}A_xCo_{1-y}M_yO_{3-\delta}$, A = Ca, Sr, Ba; M = Co, Fe, Cu, Ni) membranes have shown simultaneous occurrence of ionic and electronic conductivity [20], which makes them good candidates for catalyst in additional oxygen production in interface regions. At full density, the membrane is selectively permeable to oxygen. Oxygen diffusion coefficient can be as high as 10^{-5} cm^2s^{-1}, leading to attainable oxygen flux of the order 10^{15} to 10^{16} $cm^{-2}s^{-1}$. Operating temperatures are rather high (1100-1300 K), which may not be a setback in this application.

Adsorption of atomic oxygen on the silver membrane surface in the upstream region is relatively large, which makes the oxygen exchange coefficient relatively large in comparison with YSZ. Our experimental results have indicated that a relatively dense and thin atomic oxygen layer was formed on the silver surface [21,22]. It is assumed that the layer is formed due to strong sticking property of atomic oxygen on the silver surface. Some studies [23,24] suggested a strong dissociation of oxygen molecules on an Ag surface at a temperature close to 900 K before the oxygen adsorption process. The large concentration of atomic oxygen at the surface in turn increases the rate of oxygen permeation through the membrane.

Atomic oxygen recombines to form oxygen molecules on the other side of membrane in the down stream region. The rate of that process is fast and only oxygen molecules are detected by the mass spectrometer. Our measurements indicate that oxygen diffusivity is about 10^{-5} cm^2s^{-1}, corresponding to the maximum oxygen flux of 10^{16} to10^{17} $cm^{-2}s^{-1}$.

In view of the many advantages and setbacks of the groups of materials to be used in oxygen separation, we have proposed a standardized experimental setup that will measure oxygen flux at same physical conditions and same geometry from a set of materials. The scheme of the cell is shown in Figure 10. In addition to serving a test bed for oxygen separation materials, it will also help in the design in the actual oxygen separation devices.

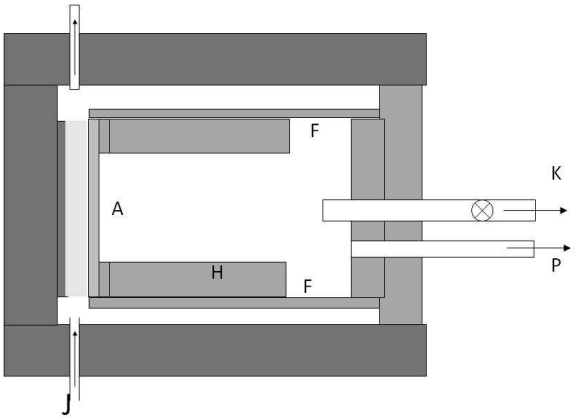

Figure 10. Oxygen separation test cell: A – diffusion membrane, H – heater, F - thermal shield, K - to mass spectrometer/inflatable oxygen container, P – to pressure gauge, J - Martian entry simulant mixture (in/out),.

(7) *Rigid, thermo-resistant inflatable container for oxygen/carbon dioxide storage*

Special attention will be given to tests with inflatable containers to establish a data matrix for oxygen storage conditions. Contacts with current suppliers of the inflatable structures will be made to determine the best available candidate for a rigid, thermo-resistant, inflatable oxygen container that operates effectively at mass flow rates of the Mars entry plasma. The container must be minimally intrusive, shaped so that it produces minimal addition of the drag and does not affect the motion during entry.

4. CONCLUDING REMARKS

Kinetic energy of Mars Pathfinder was about 15.2 GJ, as mentioned in the Introduction. Based on the loss in velocity, Mars Pathfinder lost about 92.5% of that energy during the plasma-sustaining entry phase that is about 14 GJ, approximately. It is interesting to note that an ideal MHD generator with fully ionized entry plasma, and a magnetic field of 1T could convert more than 7 GJ of heat released. Therefore the MHD generator absorbs more than 50% of the kinetic energy loss. That means that the heat transferred to the probe can be reduced by at least 50%. MHD conversion could be therefore acting not only as the power generating, but also as the cooling process.

We estimate that total mass of the permanent magnets should be no more than 10 to 20 kg per square meter of exposed surface. This is 1.5 to 3% of the total mass of Mars Pathfinder and presents a favorable trade-off for the reduction of heat transfer and extraction of reusable energy. Although use of permanent magnets has proved successful in the laboratory experiment, their further implementation requires proper thermal shields. In this aspect, electromagnets could be considered as an alternative, especially in view that the optimal magnetic field strength in the entry plasma is time dependent and time response of permanent magnets may not be fast enough.

Converted power distribution presents additional challenge. In the first stage, the onboard systems can be designed to use the converted power to perform a few usefull utility services, such as active cooling, redistribution of heat and powering oxygen separation devices. Martian entry plasma reflectivity does not allow transmitting the power from the spacecraft, but elaborate concepts of rigid inflatable containers and structures pulled in the wake could provide the enabling technology.

Using a relatively simple laboratory plasma flow system, we have demonstrated extraction of MHD power. The extracted power density is limited by the size of the external MHD generator models, and by the flow velocity. Compact $SmCo_5$ permanent magnets were used in the experiments successfully. Change of chemical composition of the Martian air plasma was confirmed. Taking into account the scaling factor due to difference in velocity and ionization, we were able to validate the concept by extracting the scalable power density.

5. ACKNOWLEDGEMENT

The findings reported herein could not have been possible without the contributions of Dennis Bushnell, Peter Gnoffo, Mark Saunders, Charles McClish, Robert Dillman, Warren Kelliher, David Alexander, John Cole, Sergey Macheret, Reginald Exton, John Buckley, Dale Taylor, Douglas Tolbert, Joseph Parker, Nirvana Mehan, Erin Gatling, Melanie Fox, Daniel Chattin, Juan Cruz, Will Scott, and Robert Ash, for which the authors are sincerely grateful. Help by Zhon Shi, Thao Dinh, and Jan Drake is also gratefully acknowledged.

Svetozar Popovic and Leposava Vuskovic gratefully acknowledge support of NASA Langley Research Center through ODURF Project #133931,

6. REFERENCES

1. Moses, R.W., “Regenerative Aerobraking,” *Space Technology and Applications International Forum (STAIF) 2005*, Paper No. 57, 13-17 February 2005, Albuquerque, New Mexico.

2. Spencer, D., Blanchard, R., Braun, R., Kallemeyn, P., and Thurman, S., “Mars Pathfinder Entry, Descent,

and Landing Reconstruction," *Journal of Spacecraft and Rockets*, Vol. 36, No. 3, May-June 1999.
3. Raofi, B., Bhat, R., and D'Amario, L., "Flight Path Control Strategies for the 2003 Mars Exploration Rover (MER) Mission," *AIAA-2002-4824, AIAA/AAS Astrodynamics Specialist Conference and Exhibit*, 5-8 August 2002, Monterey, California.
4. Smith, J. and Bell, J., "2001 Mars Odyssey Aerobraking," *AIAA-2002-4532, AIAA/AAS Astrodynamics Specialist Conference and Exhibit*, 5-8 August 2002, Monterey, California.
5. Lyons, D., "Mars Reconnaissance Orbiter: Aerobraking Reference Trajectory," *AIAA-2002-4821, AIAA/AAS Astrodynamics Specialist Conference and Exhibit, 5-8 August 2002*, Monterey, California.
6. David W. Way, Richard W. Powell, Karl T. Edquist, James P. Masciarelli, and Brett R. Starr, Aerocapture Simulation and Performance for the Titan Explorer Mission, *AIAA 2003-4951, 39th IAA/ASME/SAE/ASEE Joint Propulsion Conference and Exhibit*, 20-23 July 2003, Huntsville, Alabama.
7. H. Requiston, P. Augros, F. Bonnefond, JM. Bouilly, T. Lutz, H. Scheer, Aerofast: Aerocapture for Future Space Transportation, p369, *7th International Planetary Probe Workshop*, Barcelona, Spain, 14-18 June 2010.
8. J. T. Schofield, J. R. Barnes, D. Crisp, R. M. Haberle, S. Larsen, J. A. Magalhaes, J. R. Murphy, A. Seiff, and G. Wilson, *Science*, vol. 278, pp. 1752-1758 (1997).
9. D. J. Drake, S. Popović, L. Vušković, and T. Dinh, "Kinetic Description of Martian Atmospheric Entry Plasma,"*IEEE Trans. on Plasma Sci*. 37, 1646-1655 (2009).
10. L. Vuskovic, and S. Popovic, "Magnetohydrodynamic Power Generator," Summary of Research Report for *ODURF Project #133931*, March 2004.
11. Rosa, R. J., *Magnetohydrodynamic Energy Conversion*, Hemisphere Publishing Corporation, New York, 1987.
12. Sridhar, K.R., Vaniman, B.T., "Oxygen Production on Mars using Solid Oxide Electrolysis," SAE Paper 951737, 25th International Conference on Environmental Systems, San Diego, California July 1995.
13. Minh, N., Chung, B., Doshi, R., Montgomery, K., Ong, E., Reddig, M., MacKnight, A., and Fuhs, S., "Zirconia Electrolysis Cells for Oxygen Generation from Carbon Dioxide for Mars In-Situ Resource Utilization Applications," SAE Paper 981655, 1998 SAE Transactions Journal of Aerospace.
14. Brossmann, U., Würschum, R., Södervall, U. and Schaefer, H.-E., "The diffusion of oxygen in ultrafine grained, undoped monoclinic ZrO_2", *J. Appl.Phys.* **85,** 7646–7654 (1999).
15. Knöner, G., Reimann, K., Röwer, R., Södervall, U., and Schaefer, H-E., "Enhanced oxygen diffusivity in interfaces of nanocrystalline ZrO_2_Y_2O_3", *Proceedings of the National Academy of Sciences of the United States of America*, **100**, 3870-3873 (2003).
16. Kushima, A., and Yildiz, B., "Oxygen ion diffusivity in strained yttria stabilized zirconia: where is the fastest strain?", *Journal of Materials Chemistry*, **20**, 4809-4819 (2010).
17. Kim, B.-K., Park, S.-J. & Hamaguchi, H. , *J. Am. Ceram. Soc.* **76**, 2119–2122 (1993).
18. Williams, S., Popović, S., and Gupta, M., "Microwave plasma generation and filtered transport of O_2 (a $^1\Delta_g$)," *Plasma Sources Science and Technology* **18**, 035014 (2009).
19. Chen, C.S., Kruidhof, H., Bouwmeester, H.J.M., Verweij, H., and Burggraaf, A.J., "Thickness dependence of oxygen permeation through erbiastabilized bismuth oxide-silver composites", *Solid State Ionics*, **99**, 215 (1997).
20. Teraoka , Y., Nobunaga, T., Okamoto, K., Miura, N., and Yamazoe, N., "Influence of constituent metal Cations in substituted $LaCoO_3$ on mixed conductivity And oxygen permeability," *Solid State Ionics*, **48**, 207 (1991).
21. Wu, D., Outlaw, R. A., and Ash, R. L., "Glow-discharge enhanced permeation of oxygen through silver", *J. Appl. Phys.*, **74**, 4990 (1993).
22. Vušković, L., Ash, R. L., Shi, Z., Popović S. , and Dinh, T., "Radio-Frequency-Discharge Reaction Cell for Oxygen Extraction from Martian Atmosphere," Transactions of the Society of Automotive Engineers, J. of Aerospace, **106**, 1041-1047 (1998).
23. Butler, D. A., Sanders, J. B., Raukema, A., Kleyn, A. W., and Frenken, J. M., "Oxygen dissociation on Ag (110), *Surface Science*, **375**, 141 (1997).
24. Wang, J.-H., Dai, W.-L., Deng, J.-F., Wei, X.-M., Cao, Y.-M., Zhai, R.- S, "Interaction of oxygen with silver surface at high temperature", *Applied Surface Science*, **126**, 148 (1998).